

RTI Goes Wild: Radio Tomographic Imaging for Outdoor People Detection and Localization

Cesare Alippi, *Fellow, IEEE*, Maurizio Bocca, Giacomo Boracchi,
Neal Patwari, *Fellow, IEEE* and Manuel Roveri

Abstract—In recent years, Radio frequency (RF) sensor networks have been used to localize people indoor without requiring them to wear invasive electronic devices. These wireless mesh networks, formed by low-power radio transceivers, continuously measure the received signal strength (RSS) of the links. Radio Tomographic Imaging (RTI) is a technique that generates, starting from these RSS measurements, 2D images of the change in the electromagnetic field inside the area covered by the radio transceivers to spot the presence and movements of animates (*e.g.*, people, large animals) or large metallic objects (*e.g.*, cars). Here, we present a RTI system for localizing and tracking people outdoors. Differently than in indoor environments where the RSS does not change significantly with time unless people are found in the monitored area, the outdoor RSS signal is time-variant, *e.g.*, due to rainfalls or wind-driven foliage. We present a novel outdoor RTI method that, despite the nonstationary noise introduced in the RSS data by the environment, achieves high localization accuracy and dramatically reduces the energy consumption of the sensing units. Experimental results demonstrate that the system accurately detects and tracks a person in real-time in a large forested area under varying environmental conditions, significantly reducing false positives, localization error and energy consumption compared to state-of-the-art RTI methods.

Index Terms—radio tomography, device-free localization, wireless sensor networks, adaptive systems

I. INTRODUCTION

IN this paper, we consider the problem of detecting, localizing and tracking people not wearing/carrying an electronic device, thus not actively participating in the localization effort, in large and heavily obstructed outdoor environments. To this purpose, we use an RF sensor network, *i.e.*, a wireless system composed of low-power, inexpensive commercial off-the-shelf radio transceivers operating in the 2.4 GHz ISM band [1]. These devices form a wireless mesh network by continuously broadcasting packets and measuring the received signal strength (RSS) of the network links. Radio tomographic imaging (RTI) [2] techniques process the RSS measurements collected by the RF sensors on multiple frequency channels [3] and generate 2D images of the changes in the electromagnetic field over the deployment area due to the presence and movements of animates (*e.g.*, people, large animals) or metallic objects (*e.g.*, cars [4]). By further processing these images,

the targets can be accurately detected and tracked [5]. Our work introduces an accurate and energy-efficient RTI method that successfully deals with the nonstationary noise introduced in the RSS measurements by environmental factors, such as rainfalls or wind-driven foliage, typically encountered in real-world outdoor environments.

RF sensor networks represent an appealing technology for detecting and tracking people outdoors: due to the small size and low cost of the RF units, they are less invasive and better conceivable than video camera networks, and considerably less expensive than ultra-wideband (UWB) transceivers. They also work in the dark and through smoke and non-metallic walls. However, an RF sensor network deployed outdoors has to face challenging conditions, different from the more static ones typically found in real-world indoor environments [6]. The main challenges encountered in outdoor environments are:

- The presence of what we refer to as *environmental noise*, *i.e.*, the significant variation in RSS observed when no person is located in the monitored area due to the time-varying multipath introduced by *e.g.* wind-driven foliage, rainfalls or snow. In homes and buildings, on the contrary, the RSS is measured in quasi stationary conditions and does not vary significantly with time: spurious variations in indoor conditions can be introduced by overlapping Wi-Fi networks increasing the floor noise level of the radio channel [7].
- The *lack of an initial calibration* of the system performed in stationary conditions. Due to the intrinsic nonstationarity of the outdoor environment, RTI methods can not rely on an initial calibration to estimate the average RSS of the links of the network, which is then used as a reference to calculate the change in the electromagnetic field introduced by the presence of people in the monitored area.
- The need to address the *energy efficiency* of the system. The remote locations and harsh weather conditions drive the need for a battery powered capability of the RF sensors, which, in turn, requires the adoption of an adaptive radio duty cycling mechanism to extend the lifetime of the system or, when energy harvesting systems are enforced [8], reduce their cost and size.

Several application scenarios could take advantage of an RF sensor network for outdoor people detection and localization. For example, in natural parks populated by protected animal species, a system composed of small and covert devices could be used to detect and locate poachers even in areas

Cesare Alippi, Maurizio Bocca, Giacomo Boracchi and Manuel Roveri are with the Dipartimento di Elettronica, Informazione e Bioingegneria, Politecnico di Milano, Milan, Italy. E-mail: firstname.lastname@polimi.it. Neal Patwari is with the Department of Electrical and Computer Engineering, University of Utah, and with Xandem Technology, both in Salt Lake City, UT, USA. E-mail: npatwari@ece.utah.edu

characterized by a dense canopy, which can not be monitored *e.g.* with air surveillance [9]. An outdoor RTI system could be used to monitor long international borders running across heavily forested areas from people trying to *e.g.* smuggle drugs or weapons, to protect large vineyards from vandalism or theft, or to create a virtual fence at a pasture site [10] that would not require the cattle to wear GPS collars. Besides security and perimeter surveillance applications, an RTI system would greatly extend the capabilities of *smart spaces* such as university campuses, malls and hospitals.

In this work, we introduce a novel RTI method for outdoor environments achieving high detection and localization accuracy and improving the overall system's energy efficiency. The main contributions of our work can be summarized as follows:

- We characterize the relationship existing in nonstationary outdoor environments between the variation in RSS due to environmental noise and the link's *fade level* [11], *i.e.*, the difference between the measured and theoretical RSS of a link (see Section III-A).
- We propose a method for selecting those link-frequency channel combinations (which we refer to as *link-channel pairs*) that, even in nonstationary environmental conditions, appear to be the most reliable for detecting the presence of a person on the link line, *i.e.*, the imaginary straight line connecting transmitter and receiver (see Section III-B). We verify that this selection method allows enhancing both the detection and localization accuracy while simultaneously reducing the system's energy consumption.
- We introduce an adaptive method (see Section III-C) to recalibrate on-line the reference RSS of the selected link-channel pairs, even in presence of environmental noise and people in the monitored area, and apply a background subtraction technique (see Section III-E) on the estimated radio tomographic images to further increase the robustness of the system to time-varying environmental noise.

The performance of the outdoor RTI method was evaluated in a set of experiments carried out in a challenging outdoor environment, *i.e.*, a $35m \times 60m$ heavily forested area with trees and bushes of various height, shape and size. Tests were performed in different environmental conditions (*e.g.*, with no wind, light breeze, or gusts of wind). False alarm rate, localization accuracy and energy efficiency associated with the novel method are compared to those of the RTI methods originally introduced in [5], [12], to date the most accurate RTI methods used in indoor environments, which we suitably adapt to the considered outdoor scenario in order to make a fair comparison. Experimental results demonstrate that the novel outdoor RTI method keeps under control the false positive and negative rates (0.04% and 0%, respectively), and reduces both the localization error (from 20% to 46%) and the energy consumption of the whole system (from 62% to 87%) compared to state-of-the-art methods.

The paper is organized as follows. In Section II, we survey the related literature on people detection and localization in outdoor environments and on state-of-the-art RTI methods. The novel outdoor RTI method is presented in Section III,

while the experimental setup is described in Section IV. Section V lists the metrics used to evaluate the performance of the system. The results of the tests are presented in Section VI. Conclusions are given in Section VII.

II. RELATED LITERATURE

The problem of localizing and tracking people in large outdoor areas has been addressed by several works. The system in [13] was composed of spatially distributed Radio-frequency identification (RFID) readers measuring the RSS of RFID tags carried by people moving in the monitored area. The position of the targets was estimated by using a RSS-distance model whose parameters were calibrated on-line to make the system more robust to environmental changes. The work in [14] presented a heterogeneous system composed of low-quality wireless camera nodes devoted to people localization and RFID readers devoted to identification. Both the systems in [13] and [14] assumed that the targets to be located were carrying an RFID tag. Device-free localization and tracking of people has often been carried out by using visual sensor networks [15], *i.e.*, wireless systems composed of a large number of low-power camera nodes. However, cameras produce a large amount of image data for the limited network's resources. In addition, cameras suffer from poor light conditions and occlusions in cluttered outdoor environments (such as *e.g.* forested areas). For these reasons, other works have proposed using radars to detect personnel in heavily wooded areas. In [16], [17], micro-Doppler signals, *i.e.*, Doppler scattering returns not due to gross translation of the target but are instead produced by the periodic movements (*e.g.*, of legs or arms) of a walking human target, are exploited for detecting humans and distinguishing them from other animals. However, stand-alone low-frequency radars have a poor angular resolution. To overcome this limitation, the work in [18] proposes a multiple-input multiple-output (MIMO) radar exploiting the angular diversity of spaced antennas to detect the changes in the RF channel due to personnel in the deployment area. In this work, we present an energy-efficient RTI method that enables device-free detection, localization and tracking of people in large and cluttered outdoor areas covered by a small number of low-cost and low-power RF sensors.

The impact of environmental factors on wireless sensor networks deployed outdoors has been previously investigated. The works in [19], [20] analyze how the density and seasonal variations of vegetation, and daily temperature/humidity fluctuations affect the RSS and the links connectivity. The work in [21] studies how wind, *i.e.*, wind-driven vegetation movement, affects the propagation of radio signals at different frequencies (0.9, 2, 12, and 17 GHz). Experimental data demonstrate that the variation in RSS increases with the wind speed (more consistently at higher frequencies) and that the fade distribution goes from being Rician to being Rayleigh with an increasing wind speed. However, these works did not consider the combined effect of environmental factors and animates on the measured RSS.

Different RTI methods were introduced in [2], [22], [23], [24]. In [3], frequency diversity was exploited to improve the

localization accuracy. The same principle was later applied in [5], [12]. In all these works, the RTI systems were deployed in stationary indoor environments (*i.e.*, no changes in the environment nor time-varying environmental noise). The system described in [6] was deployed in a real-world domestic environment over a three months period. To recalibrate in an on-line fashion the reference RSS values of the links of the network, the RSS signals were low-pass filtered. By doing this, the system maintained a high localization accuracy (0.3 m approximately) despite the frequent changes in the environment. In [25], the authors carried out tests in a through-wall scenario having some of the RF sensors located in the proximity of trees whose branches were swaying in the wind. They proposed a subspace decomposition method to separate the change in RSS due to human motion from that introduced by environmental noise. However, the amount of variation in the RSS signals due to the environment was estimated during an initial calibration performed with no person in the deployment area. Thus, the method assumed that the spatial and temporal characteristics of the environmental noise were constant. Such an assumption can not be made in a forested outdoor environment, where the environmental noise is highly time-varying.

The RTI methods described above did not consider the issue of energy efficiency: the nodes radio, *i.e.*, the most energy-hungry component, was always on, being the nodes in receive mode at all times, except for when they were transmitting a packet. Energy efficient methods were presented in [26], [23], [27]. In [26], the authors apply compressed sensing techniques to RTI, reducing the number of links that have to be sampled in order to reconstruct the whole image. In [23], an accurate time synchronization protocol is used to enable radio duty cycling. In [27], only the links near the current location of the tracked targets are measured. In our work, we present a method to select those link-channel pairs that are robust to environmental noise (thus, the most informative and reliable for RTI). This approach allows increasing the energy efficiency of the system, while simultaneously improving its detection and localization performance.

III. OUTDOOR RTI

This section describes the proposed outdoor RTI method. We provide the basics of RTI, focusing on the solutions developed to address the challenges posed by multipath-rich and time-varying outdoor environments. The reader is invited to refer to [2], [3], [12], [22], [28], [29] for a detailed description of the principles of RTI. Algorithm 1 details the novel outdoor RTI method.

A. Links Characteristics in Nonstationary Environments

First, we analyze the characteristics of the links in nonstationary outdoor environments. To do this, we use the concept of fade level introduced in [11], which defines the relationship between steady-state, narrow-band fading and the changes in RSS due to a person crossing the link line. The fade level of link l on channel c , $F_{l,c}$, can be estimated as:

$$F_{l,c} = \bar{r}_{l,c} - P(d_l), \quad (1)$$

Algorithm 1: Outdoor RTI method

input : N static RF sensors located at (estimated) positions $\{x_n, y_n\}_{n=1, \dots, N}$
 Communicating on a set of different frequency channels \mathcal{C}
 Measuring the RSS on the link-channel pairs of the network.

output: $\hat{\mathcal{P}}(k)$ (estimated positions of the people found in the monitored area at time k)

- 1 Calculate the projection matrix $\mathbf{\Pi}$
- while** (1) **do**
 - 2 **At the completion of each full TDMA cycle:**
 Update the reference RSS $\bar{r}_{l,c}(k)$ of the selected link-channel pairs
 Estimate the change in RSS y_l of the selected link-channel pairs
 Estimate the radio tomographic image $\hat{\mathbf{x}} = \mathbf{\Pi} \mathbf{y}$
 Apply background subtraction to $\hat{\mathbf{x}}$ and update the background image
 Apply target detection and tracking method to estimate $\hat{\mathcal{P}}(k)$
 - 3 **Every ΔT_N hours:** (*e.g.*, $\Delta T_N = 2$)
 Measure the RSS of all link-channel pairs $\{l, c\}$ of the network for ΔT_c minutes (*e.g.*, $\Delta T_c = 5$)
 Estimate fade level, $F_{l,c}$, and RSS variance, $\sigma_{l,c}^2$, of the link-channel pairs
 Select the most reliable link-channel pairs to be used for RTI
- 4 **end**

where:

$$P(d_l) = P_0^n - 10\eta_n \log_{10} \left(\frac{d_l}{d_0^n} \right). \quad (2)$$

In (1), $\bar{r}_{l,c}$ is the average RSS of link l on channel c measured with no person in the proximity of the link line, and $P(d_l)$ is the theoretical RSS, predicted by using the log-distance path loss model [30], for two nodes at distance d_l . The equation in (2) represents a *node-specific* log-distance path loss model whose parameters η_n , P_0^n and d_0^n (*i.e.*, the path loss exponent, reference path loss, and reference distance, respectively), are derived by fitting the average RSS of those links having node n as transmitter. In other works, *e.g.*, [12], a global path loss exponent was estimated by fitting the average RSS of all the links of the network. In this work, by generating for each RF sensor an individual distance-RSS model, hardware variability factors (such as *e.g.* antenna impedance matching or relative antenna orientation between transmitter and receiver [31]) and local environmental differences (such as *e.g.* the proximity to the node of dense foliage) are taken into consideration [32]. In Section VI, we show that, by deriving an individual model for each node instead of a global one, the system achieves better detection and localization performance.

The fade level can be interpreted as a measure of whether a link-channel pair is experiencing destructive or constructive multipath interference (or not): in the first case, the fade level is negative and the link-channel pair is said to be in *deep fade*;

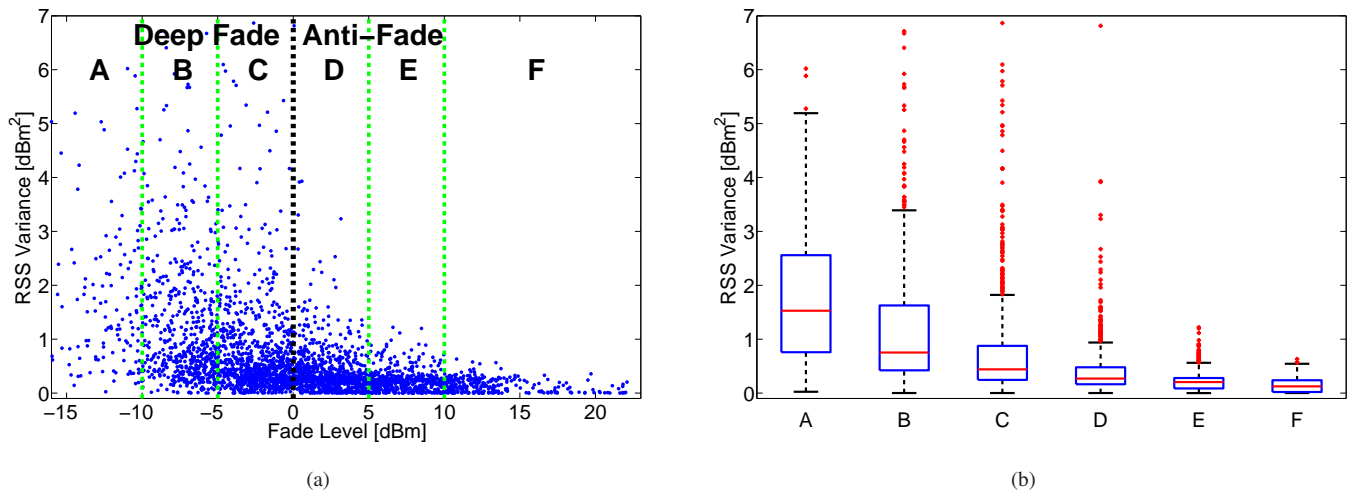


Fig. 1. Fade level vs. RSS variance due to environmental noise. The points in Figure (a) are obtained by measuring the RSS of all the link-channel pairs of the network during four intervals of 15 minutes with wind of varying intensity blowing in the deployment area. Figure (b) shows the boxplots of the distribution of the RSS variance of the link-channel pairs divided in sub-groups (A-F in Figure (a)) based on their fade level. On each box, the central bar represents the median of the distribution, the edges are the 25th and 75th percentiles, and the external points are meant to identify outliers, which are plotted individually.

in the latter case, the fade level is positive and the link-channel pair is said to be in *anti-fade*. However, even in multipath-rich indoor environments, the measured RSS does not vary significantly unless, *e.g.*, a human body affects the propagation of one (or more) of the multipath components. On the contrary, outdoor environmental factors, such as wind, rainfall or snow, introduce a significant variation in RSS even when no person is found in the deployment area. We measure the effect of the environmental noise on a link-channel pair as the variance of the RSS measurements collected when no person is in the proximity of the link line. The relationship between fade level and environmental noise is depicted in Figure 1. The points in Figure 1(a) are obtained by measuring the RSS of all the link-channel pairs of the system described in Section IV during four different intervals of 15 minutes with wind of varying intensity blowing in the deployment area. Figure 1(b) shows the boxplot of the RSS variance of all the link-channel pairs, divided in six sub-groups (A-F) based on their fade level. The data show that link-channel pairs in deep fade, *i.e.*, those having negative fade level, have a higher RSS variance when the wind becomes stronger. Thus, those links hardly contribute to the detection and localization problems.

Data in Figure 1 show that link-channel pairs with a positive fade level (*i.e.*, in anti-fade) are more robust to environmental noise. Moreover, link-channel pairs in anti-fade are characterized by a smaller sensitivity area [11], [12], *i.e.*, the area where a person affects the RSS. This area is modeled as an ellipse having transmitter and receiver at the foci [28]: for link-channel pairs in anti-fade, it can be modeled as a *narrow* ellipse around the link line. Thus, link-channel pairs with a positive fade level are not only more robust to environmental noise but can also be considered more reliable indicators of the presence of a person in the proximity of the link line. We provide an example of this in Figure 2, which shows the RSS, measured on different frequency channels, of a 25 m link

cutting through several branches of the trees found in the area. During the test, carried out in a day with wind of moderate intensity, a person crossed the link line at $t = 282$ s. The only channel in anti-fade, *i.e.*, channel 26 having $F_{l,c} = 2.1$ dBm, measured a consistent attenuation (12 dBm) in RSS at the crossing event, while exhibiting small variation in RSS due to the movements of the wind-driven foliage. On the contrary, the other two channels in deep fade show a continuous, significant variation in RSS due to the action of the wind, and this does not allow to unequivocally detect the crossing event.

B. Link-Channel Pairs Selection

We now present a method to select a subset of link-channel pairs to be used for RTI. The reason for doing this is twofold: on one hand, we want to select link-channel pairs that are more robust to environmental noise and, at the same time, more informative about the position of the targets in order to enhance the detection and localization performance of the system. On the other, we want to increase the energy efficiency of the system, since the radio of the RF sensors can be turned off during the TDMA slots originally allocated to the discarded link-channel pairs.

Define \mathcal{L}_p to be the set of link-channel pairs with positive fade level

$$\mathcal{L}_p = \{(l, c) : F_{l,c} > 0\}, \quad (3)$$

where l is the link and c the frequency channel.

Due to the low nodes density typical of outdoor deployments and the presence of several obstructions, some link-channel pairs may measure a RSS close to the sensitivity threshold of the radio modules (-97 dBm at typical ambient temperatures for the radios described in Section IV-A). Links with an average RSS close to the sensitivity threshold belong to a *grey region* [33] in which their connectivity performance becomes highly unpredictable and their RSS measurements include

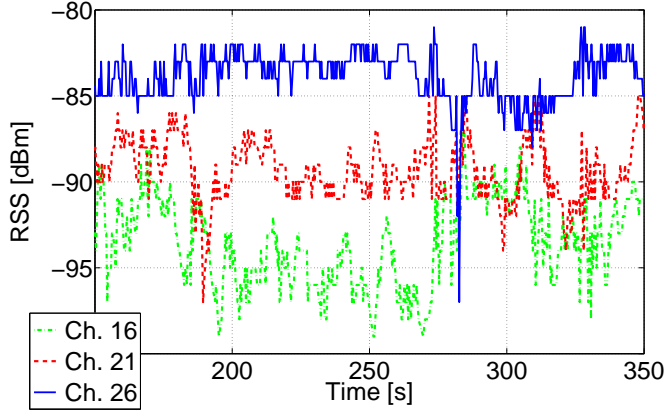


Fig. 2. The RSS, measured on different frequency channels, of a 25 m link cutting through several branches of trees found in the area of the test. During the test, carried out in a day with wind of moderate intensity, a person crossed the link line at $t = 282$ s.

noise and interference due to very weak signals. Moreover, the connectivity of these links is highly affected by changes in the environment [34]. Thus, we discard all link-channel pairs with an average RSS lower than a pre-defined threshold Υ_r (we set $\Upsilon_r = -90$ dBm).

Define \mathcal{L}_r to be the set of link-channel pairs with average RSS higher than Υ_r

$$\mathcal{L}_r = \{(l, c) : \bar{r}_{l,c} > \Upsilon_r\}. \quad (4)$$

Now define $\mathcal{L}_s = (\mathcal{L}_p \cap \mathcal{L}_r)$ to be the set of link-channel pairs to be considered. Both the fade level and the average RSS of the link-channel pairs are estimated when no person is found in the deployment area.

For each link-channel pair, we calculate a weight $\rho_{l,c}$ as follows

$$\rho_{l,c} = \begin{cases} F_{l,c}/\sigma_{l,c}^2 & \text{if } (l,c) \in \mathcal{L}_s \\ 0 & \text{otherwise} \end{cases}, \quad (5)$$

where $\sigma_{l,c}^2$ is the RSS variance measured when no person is found in the deployment area. Consequently, link-channel pairs having low RSS variance are assigned a higher weight, since the variations in RSS measured on such links have a higher probability of being human-induced.

Finally, define the set \mathcal{L} as

$$\mathcal{L} = \left\{ (l, c) : (l, c) \in \mathcal{L}_s \wedge c = \max_{j \in \mathcal{C}} \rho_{l,j} \right\}, \quad (6)$$

i.e., as the set in which, for each link in \mathcal{L}_s , only the frequency channel in \mathcal{C} (where \mathcal{C} represents the set of measured frequency channels) characterized by the largest weight is included.

C. RSS Change Estimation

The change in RSS at time k for each link-channel pair in \mathcal{L} is estimated as:

$$y_{l,c} = |r_{l,c}(k) - \bar{r}_{l,c}(k)|, \quad (7)$$

where $r_{l,c}(k)$ and $\bar{r}_{l,c}(k)$ are the *measured* and *reference* RSS of the link-channel pair (l, c) , both considered at time

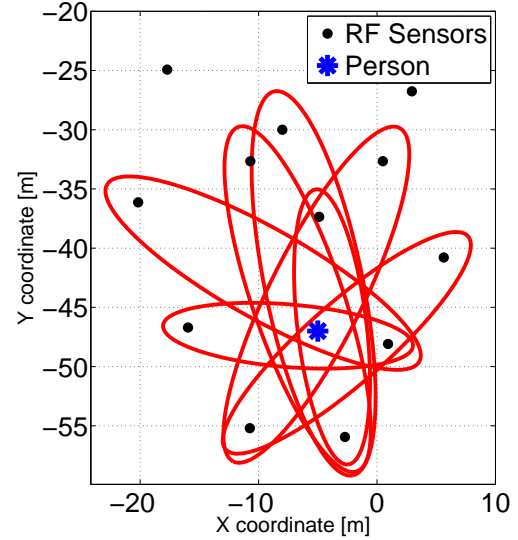


Fig. 3. At time k , the FIFO buffers of the selected link-channel pairs whose sensitivity areas (red ellipses) include a person's estimated position are not updated. The FIFO buffers of the other selected link-channel pairs are instead updated. For each link-channel pair in \mathcal{L} , the reference RSS is calculated as the average of the RSS measurements contained in its FIFO buffer.

k , respectively. In most of the previous works (*e.g.*, [2], [5], [12]), the reference RSS was calculated as the average RSS measured during an initial calibration of the system carried out in absence of people in the monitored area. This approach showed to be effective in stationary indoor environments. In [6], the reference RSS was estimated in real-time by low-pass filtering the measured RSS. This approach was effective in a dynamic domestic environment characterized by frequent, bursty events modifying the attenuation field of the deployment area. However, this approach was not effective when the person to be localized was not moving for an extended period of time (*e.g.*, sleeping): in that case, the reference RSS quickly converged to the measured RSS, bringing the corresponding change in RSS to zero despite the presence of the person in the deployment area. Due to the presence of a time-varying environmental noise affecting the RSS measurements, an outdoor RTI system must continuously update the reference RSS of the selected link-channel pairs, even when people are not moving inside the deployment area.

To estimate the reference RSS in real-time without losing people who stop moving, we use the following procedure. We first create, for each selected link-channel pair, a FIFO buffer of $N_w = \lfloor T_w/T_s \rfloor$ elements. T_w is the length of the considered time window (*e.g.*, $T_w = 5$ s) and T_s is the sampling interval of the RTI system, *i.e.*, the interval of time required by the system to complete all the TDMA rounds of communication on the frequency channels in \mathcal{C} (see Section IV-A). Define $\hat{\mathcal{P}}(k)$ to be the set of estimated positions at time k of the people located in the deployment area ($\hat{\mathcal{P}}(k) = \emptyset$ if no person is in the deployment area). Since the change in RSS of a link is assumed to be a spatial integral of the attenuation field of the monitored area, only the attenuation in the elliptical

sensitivity area of the link will affect its RSS. Thus, at time k , only the FIFO buffers of link-channel pairs whose sensitivity areas do not include one of the positions in $\hat{\mathcal{P}}(k)$ are updated. For each link-channel pair in \mathcal{L} , the reference RSS $\bar{r}_{l,c}(k)$ is calculated as the average of the RSS measurements contained in its FIFO buffer. In this way, the system does not require an initial calibration to calculate the reference RSS. Moreover, the reference RSS does not converge to the measured RSS even when the person stops moving for an extended period of time.

D. Radio Tomographic Image Estimation

When we consider all the $N(N - 1)$ links of the network, the relation between the change in the electromagnetic field of the deployment area \mathbf{x} and the measured RSS changes \mathbf{y} is modeled as:

$$\mathbf{y} = \mathbf{W}\mathbf{x} + \mathbf{n}, \quad (8)$$

where \mathbf{y} and \mathbf{n} are vector of size $N(N - 1)$ of the RSS change and noise of the links of the network, respectively. For the links belonging to \mathcal{L} , the RSS change is calculated as in (7). For all the others, the RSS change is zero. Vector \mathbf{x} represents the change in the *discretized* electromagnetic field of the monitored area, *i.e.*, the intensity of each pixel of the radio tomographic image to be estimated. Thus, \mathbf{x} is a vector of size P , where P is the total number of pixels of the radio tomographic image. Element $w_{l,q}$ of the weight matrix \mathbf{W} (of size $N(N - 1) \times P$) indicates how pixel q affects the change in RSS of link l . Since the sensitivity area of a link is modeled as an ellipse [28], $w_{l,q}$ is computed as:

$$w_{l,q} = \begin{cases} \frac{1}{A_l} & \text{if } d_{l,q}^{TX} + d_{l,q}^{RX} < d_l + \lambda, \\ 0 & \text{otherwise} \end{cases}, \quad (9)$$

where A_l is the area of the ellipse, *i.e.*, the sensitivity area of link l , $d_{l,q}^{TX}$ and $d_{l,q}^{RX}$ are the distances of pixel q from the transmitter and receiver, respectively, and λ is the parameter defining the width of the sensitivity area. The linear model in (8) is based on the correlated shadowing models in [2], [28], [29].

Regularization [35] is required to solve the ill-posed problem of estimating the intensity of the *many* pixels in \mathbf{x} from the *few* links' measurements in \mathbf{y} . We apply the regularized least square approach used also in [5], [12]:

$$\hat{\mathbf{x}} = \mathbf{\Pi}\mathbf{y}. \quad (10)$$

where:

$$\mathbf{\Pi} = (\mathbf{W}^T\mathbf{W} + \mathbf{C}_x^{-1}\alpha_r)^{-1}\mathbf{W}^T. \quad (11)$$

α_r is the regularization parameter (*e.g.*, $\alpha_r = 0.1$). The a priori covariance matrix \mathbf{C}_x is calculated using an exponential spatial decay model [28]:

$$\mathbf{C}_x[i, j] = \sigma_x^2 e^{-d_{i,j}/\delta_c}, \quad (12)$$

where σ_x^2 is the variance at each pixel, $d_{i,j}$ is the Euclidean distance between pixels i and j , and δ_c is a pixels' correlation distance parameter. In practice, the inversion matrix $\mathbf{\Pi}$ does not depend on the environmental conditions and needs to be calculated only once after the deployment. Thus, $\hat{\mathbf{x}}$ in (10) can be estimated in real-time.

TABLE I
RTI PARAMETERS (DEFAULT VALUES)

Parameter	Value	Description
Υ_r	-90	Link connectivity threshold [dBm]
T_w	5	Link RSS FIFO buffer length [s]
λ	2	Link ellipse (sensitivity area) width
T_b	5	Background image training period [s]
K_b	1	Background/Foreground pixel threshold
α_r	0.1	Regularization parameter
σ_x^2	0.001	Pixels' intensity variance
δ_c	1	Pixels' correlation distance
p	0.65	Pixel width [m]

E. Background Subtraction

When the process described in Section III-D is repeated over time, the estimated images $\hat{\mathbf{x}}(\cdot)$ can be considered as the *frames* of a video in which the targets, *i.e.*, the people to be tracked, move. Therefore, background subtraction techniques [36], [37], which are widely used in machine vision to detect and track moving objects in videos recorded by static cameras, can be leveraged to exploit the temporal continuity of RTI frames and improve the detection and tracking of people entering and moving in the monitored area. We model each pixel of the background (reference) image as a realization of a Gaussian distribution $\mathcal{N}(\mu_p(k), \sigma_p^2(k))$, where $\mu_p(k)$ and $\sigma_p(k)$ are the mean and standard deviation of the intensity of pixel p at time k . These parameters are computed using their sample estimators from the corresponding FIFO buffers containing $N_b = \lfloor T_b/T_s \rfloor$ elements for each pixel. At time k , the background image $\mathbf{M}(k)$ is calculated as:

$$\mathbf{M}(k) = [\mu_1(k), \dots, \mu_P(k)]. \quad (13)$$

Thus, the P -dimensional vector \mathbf{M} is initialized as the estimate of the electromagnetic field computed when no person is inside the monitored area. The background subtracted radio tomographic image, $\hat{\mathbf{x}}_b(k)$, is then defined as:

$$\hat{\mathbf{x}}_b(k) = \hat{\mathbf{x}}(k) - \mathbf{M}(k), \quad (14)$$

and only those pixels in $\hat{\mathbf{x}}_b(k)$ reporting a significantly large difference are labeled as *foreground*, thus considered as potential moving objects, *i.e.*, people.

However, in nonstationary outdoor environments where the RSS signals typically change, either gradually or suddenly, the background image needs to be constantly updated. To update the background image $\mathbf{M}(k)$, we define as in [36] the set of background pixels $\mathcal{B}(k)$ from the k -th frame as:

$$\mathcal{B}(k) = \left\{ q : \frac{|\hat{\mathbf{x}}_q(k) - \mu_q(k-1)|}{\sigma_q(k-1)} \leq K_b \right\}, \quad (15)$$

where K_b is a threshold defining the confidence interval of the intensity of the pixels (we set $K_b = 1$) and $\mu_q(k-1)$ and $\sigma_q(k-1)$ are the background estimates in the previous frame $k-1$. At time k , only the pixels in $\mathcal{B}(k)$ are updated and replaced by the current estimates from the corresponding FIFO buffer, while the others are left untouched. This simple, yet effective background update method allows increasing the difference in intensity between the pixels of the blobs corresponding to real people and those of the blobs introduced

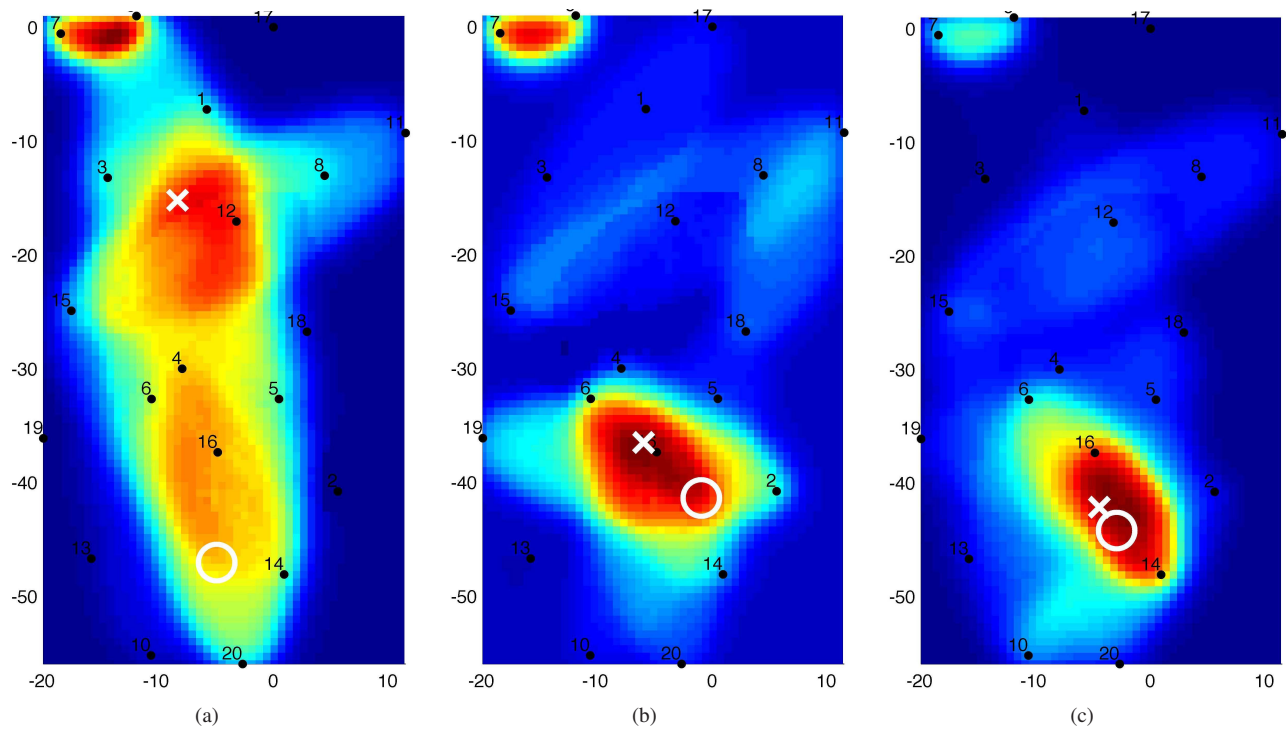


Fig. 4. Comparing radio tomographic images estimated with different methods. In (a), the image estimated with the RTI method introduced in [5] (RFL^f in Section VI-C). In (b), the image estimated with the RTI method introduced in [12] (FLB^U in Section VI-C). In (c), the image estimated with the novel outdoor RTI method presented in this work (OUT^W in Section VI-B). In the images, the white circle represents the true position of the person, while the white cross represents his estimated position. The outdoor RTI method achieves better localization accuracy and reduces the size and intensity of the spurious blobs in the image introduced by environmental noise, thus facilitating the target tracking process.

by the environmental noise, facilitating the blobs tracking problem addressed in the next section.

F. People Detection and Tracking

After estimating the image \hat{x}_b , we finally have to detect and track the blobs corresponding to real people. In order to fairly evaluate the performance of the outdoor RTI method presented in this work and compare it to previous works, we apply the multiple target tracking method in [5], which provides high accuracy (0.5 m tracking error approximately) and real-time performance with multiple people even when these have intersecting trajectories. We refer the reader to [5] for a detailed description of the applied multiple target tracking method. We emphasize that the computations required for estimating the radio tomographic image and detecting and tracking the blobs corresponding to real people can be executed in real-time on a standard PC or laptop. The parameters of the method presented in Section III are summarized in table I.

IV. EXPERIMENTAL SETUP

A. Hardware and Communication Protocol

In our experiments, we use TI CC2531 nodes [38], equipped with a SWRU120b antenna [39]. The CC2531 has a nominal maximum transmit power of 4.5 dBm, and can transmit on one of 16 frequency channels, which are 5 MHz apart, in the 2.4 GHz ISM band. Other frequency bands, *e.g.*, 900 MHz and 433 MHz, could be similarly used for outdoor RTI.

An analysis of the performance of different frequency bands for RF-based people localization in outdoor environments is outside the scope of this paper and is left for future research. The nodes used in the experiments drain approximately 35 mA when the radio is on and 20 μ A when off.

The RF sensors run a multi-channel TDMA communication protocol [40] in which each node has a unique slot number, and transmits only during its slot. Differently than in typical indoor environments where the mesh network formed by the RF sensors is fully connected, in outdoor deployments some nodes may not receive packets transmitted by other nodes, and the connectivity of links (particularly those in the grey region [33]) may vary significantly over time. The nodes use the information included in the received packets, *i.e.*, ID of the transmitting node and total number of nodes in the network, to synchronize their TX/RX schedules and synchronously switch on the next frequency channel. This mechanism does not require a command from a central coordinating unit, making the system robust both to lossy links and nodes' failure. The transmitted packets contain also the RSS of the most recent packets received from the other nodes. In our experimental setup, a sink node listens to all the packets transmitted by the nodes. The sink node is connected to a laptop where the RSS measurements are stored for post-processing. By overhearing all the traffic, the sink node collects all the RSS measurements without additional dedicated transmissions (thus, energy consumption) by the RF sensors.

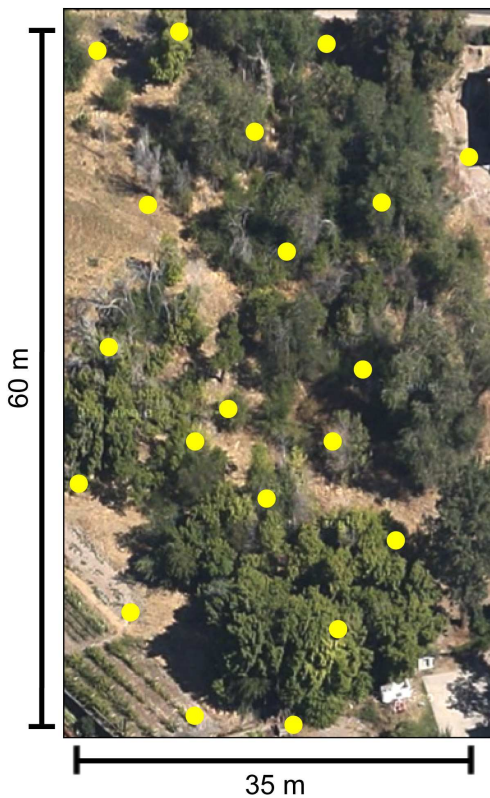


Fig. 5. Aerial view of the forested area where the experiments were carried out. The yellow circles represent the 20 RF sensors composing the RTI system, in the positions estimated by using the procedure described in Section IV-C.

B. Experiments

We perform experiments in a $35m \times 60m$ heavily forested area, shown in Figure 5. The 20 battery-powered RF sensors composing the system are attached using tape to the trunks of the trees found in the area, at different heights from the ground. The nodes communicate on four frequency channels, specifically $\mathcal{C} = \{11, 16, 21, 26\}$. The center frequency of a 802.15.4 channel is calculated as $f_c = 2400 + 5(c - 10)$ MHz, where c is the channel number. Each selected link-channel pair is measured every $T_s = 0.34$ s (*i.e.*, an approximate sampling frequency of 3 Hz). To estimate the position of the nodes, we measure at least two length-angle tuples from each sensor. Similarly, we estimate the position of other reference points throughout the deployment area. These points are used to control the movements of the person to be localized and estimate his true position during the tests.

The system runs for about eight hours, during which RSS measurements are collected with and without people moving in the monitored area. Several tests are carried out in different environmental conditions¹ (*i.e.*, absence of wind, presence of a light breeze, with moderately strong gusts of wind). The

¹During the deployment, we did not use any other sensor (*e.g.*, anemometer, temperature and humidity sensor, etc.) to measure the environmental conditions and their impact on the characteristics of the link-channel pairs. The measurements collected by these sensors could be gathered at the sink node by being included into the payload of the packets transmitted by the RF sensors (see Section IV-A). We leave this enhancement to future work.

duration of a test is approximately five minutes. In each test, a person walks in the deployment area carrying an audio recorder. The person moves along straight lines connecting the reference points and the RF sensors. Each time the person passes nearby a reference point or a sensor, he speaks into the audio recorder its ID number. In addition, the person stands without moving for some time (*e.g.*, 20 s) at various spots inside the deployment area. By interpolating the time stamps in the audio recording, we are able to always derive the true position of the person during the test.

The tests carried out during the deployment are used to evaluate the performance of the proposed outdoor RTI system in real-world, nonstationary conditions. The results are presented in section VI. We consider only the situation in which only one person at a time is located in the monitored area. However, the outdoor RTI method presented in this work can be applied to localize and track multiple people.

C. RF Sensors' Position Estimation

A RTI system is composed of N static RF sensors located at estimated positions $\{\hat{p}_x^n, \hat{p}_y^n\}_{n=1, \dots, N}$. In indoor environments, the availability of a blueprint and structural reference points enables a more precise estimation of the sensors' position. In outdoor environments, the lack of a blueprint and other reference points, the uneven terrain, and the eventual presence of trees and bushes affecting the intra-node distance measuring process increase the error in the sensors' position estimates. In a forested environment, a GPS could be used to locate the RF sensors. However, trees' canopy, trunks and dense foliage near the receiving antenna can interfere with the reception of the signals broadcasted by the satellites, causing huge positional errors, or totally block these signals, making the positioning impossible [41], [42].

We now present a method to estimate the position of the RF sensors in a forested environment in which accurate GPS positioning is unavailable. The N RF sensors are deployed at different heights from the ground, creating a mesh of link lines that conforms to the terrain undulation and capable of intersecting a human body (contrary to what happens in indoor deployments, in this case the sensors are not on the same 2D plane). We choose one sensor to be the reference one, having coordinates $(0, 0)$ in the 2D space. We proceed by manually measuring the *length* and the *angle* (relative to the North geomagnetic pole) of a limited number of links (measuring all the links would be incredibly time consuming), making sure that the measured links connect all the deployed sensors.

The initial position estimates are determined by considering only the measurements of links which sequentially connect all the deployed sensors. Starting from the initial position estimates so derived, we iteratively find the maximum likelihood estimate (MLE) of the position of each sensor by taking into consideration also the other measured links. The final position estimates of the sensors are calculated as:

$$\underset{\{\hat{p}_x^n, \hat{p}_y^n\}}{\operatorname{argmin}} \left(\frac{\sum_{l \in \mathcal{T}} (d_l - \hat{d}_l)^2}{\sigma_d^2} + \frac{\sum_{l \in \mathcal{T}} (\alpha_l - \hat{\alpha}_l)^2}{\sigma_\alpha^2} \right), \quad (16)$$

where \mathcal{T} is the set of links manually measured, d_l and α_l are the measured length and angle of the links in \mathcal{T} , respectively, and \hat{d}_l and $\hat{\alpha}_l$ are the estimated length and angle of the links in \mathcal{T} , respectively, which change at each iteration depending on the estimated positions of the RF sensors. σ_d^2 and σ_α^2 are the variance of the length and angle measurement process, respectively (we set $\sigma_d^2 = 0.5$ m and $\sigma_\alpha^2 = 5^\circ$ after collecting multiple consecutive measurements for the same links). Other methods can be considered to provide an estimate of the spatial coordinates of the sensing units, *e.g.*, see [43] for a review. We emphasize that, as mentioned above, the use of a GPS, which is in principle a viable solution, is not feasible in this scenario of heavily forested area, where the GPS signal could totally disappear or simply fade, severely affecting the localization accuracy.

V. EVALUATION METRICS

To evaluate the performance of the outdoor RTI method and of the previous methods here discussed, we use three figures of merit:

Energy efficiency coefficient: measured as the ratio of link-channel pairs that are not selected to be used for RTI, *i.e.*, the ratio of TDMA slots the nodes remain in energy-saving mode, with the radio off:

$$\vartheta_e = 1 - \frac{|\mathcal{L}|}{N(N-1)|\mathcal{C}|}. \quad (17)$$

False alarm rate: the system triggers a false alarm whenever it wrongly detects at least a person in the monitored area. We measure the false alarm rate as the percentage of radio tomographic images where the real and estimated number of people in the monitored area differ.

Localization accuracy: measured as the root mean squared error (RMSE) of the position estimates, $\hat{z}(k)$, provided by the RTI system:

$$\bar{e} = \left(\frac{1}{K} \sum_{k=1}^K (\hat{z}(k) - z(k))^2 \right)^{1/2}, \quad (18)$$

where K is the total number of position estimates provided by the system during the deployment and $z(k)$ the true position of the person at time k . We calculate the RMSE both when the person is moving, \bar{e}_m , or standing, \bar{e}_s .

VI. EXPERIMENTAL RESULTS

In this section, we first present the experimental results of the outdoor RTI method. We also consider modified versions of the original algorithm, and demonstrate that the method we propose outperforms the modified versions in terms of false alarm rate, energy efficiency and localization accuracy. Then, we evaluate state-of-the-art indoor RTI methods (*i.e.*, [5], [12]), which we suitably adapt to the considered outdoor scenario to make a fair comparison. Finally, we analyze the sensitivity of the outdoor RTI method to the parameters in Table I.

The results here presented have been obtained by considering 20 RF sensors. Larger numbers of nodes do not necessarily

provide better results, as demonstrated in [6], [44]. While more sensors provide *on average* a higher localization accuracy, both their small-scale (*i.e.*, in the order of the wavelength) position and the changing characteristics of the monitored environment can heavily affect the characteristics of the link-channel pairs, such that at times more RF sensors achieve a worse accuracy than fewer located in optimal spots.

A. Outdoor RTI Method Performance

We evaluate the performance of the outdoor RTI method by post-processing all the RSS measurements collected during the deployment of the system. The system operated for approximately 8 hours in a day with wind of varying intensity. During this time, the deployment area remained empty approximately 90% of times, while in the remaining 10% a person was present. The set \mathcal{L} of link-channel pairs selected and used for RTI is updated every two hours ($\Delta T_N = 2$ in Algorithm 1). Thus, \mathcal{L} is updated a total of four times during the deployment. Each time, the system measures the RSS of all the link-channel pairs of the network for 5 minutes. At the end of this interval, the link-channel pairs of the network are weighted and the most reliable selected. The length of the time interval ΔT_N might depend on the expected environmental conditions: smaller ΔT_N values would increase the promptness of the adaptation mechanism at the expense of an increase in the energy consumption of the RF sensors. Conversely, increasing ΔT_N might result in a decrease of the energy consumption at the expense of a possible delay in the adaptation promptness. We also comment that, besides the periodic triggering of the update procedure set by ΔT_N , we could integrate the RTI system with additional sensors (*e.g.*, temperature or humidity sensors) to actively trigger the link-channel pairs update procedure.

First, we evaluate the performance of the novel outdoor RTI method described in Section III. We name the method OUT^+ . On average, only 12.8% of the link-channel pairs are selected, *i.e.*, $\vartheta_e = 87.2\%$. When the deployment area is empty, the RTI system triggers two false alarms, detecting the presence of a person in the monitored area for 12 s, *i.e.*, a 0.04% false alarm rate. Instead, when a person is located in the monitored area area, the RMSE is $\bar{e}_m = 3.8$ m when the person is moving and $\bar{e}_s = 3.2$ m when the person does not move.

B. Modified Outdoor RTI Methods

We now evaluate the performance of modified versions of the proposed outdoor RTI method OUT^+ . First, we extend the set of selected link-channel pairs \mathcal{L} by considering for each link $l \in \mathcal{L}_s$ the RSS measurements collected on all the selected frequency channels (instead of considering only the frequency channel having the highest weight $\rho_{l,c}$). In this version of the outdoor RTI method (which we name OUT^w), the change in RSS for link l at time k is calculated as:

$$y_l(k) = \frac{\sum_{c \in \mathcal{L}_s} \rho_{l,c} |r_{l,c}(k) - \bar{r}_{l,c}(k)|}{\sum_{c \in \mathcal{L}_s} \rho_{l,c}}, \quad (19)$$

i.e., as the weighted average of the change in RSS measured on the selected frequency channels. This method that merges the RSS data collected for the same link on different frequency

TABLE II
SUMMARY OF THE PERFORMANCE OF OUTDOOR RTI METHODS

METHOD	PATH LOSS EXPONENT		LINK-CHANNEL SELECTION		PERFORMANCE			
	Node-specific	Global	Heaviest channel	Weighted average	ϑ_e	False alarm rate [%]	\bar{e}_m [m]	\bar{e}_s [m]
OUT^+	✓		✓		87.2	0.04	3.8	3.2
OUT^w	✓			✓	67.2	0.07	3.7	3.2
COM^+		✓	✓		88.3	0.06	5.0	4.2
COM^w		✓		✓	68.7	0.07	4.9	4.1

channels was originally introduced (in an indoor localization context) in [5]. With OUT^w , the system selects on average 32.8% of the link-channel pairs, i.e., $\vartheta_e = 67.2\%$, and has a 0.07% false alarm rate (two triggered false alarms, person detected in the deployment area for 18 s). The RMSEs are $\bar{e}_m = 3.7$ m and $\bar{e}_s = 3.2$ m. Thus, the neglectable 0.1 m improvement in \bar{e}_m of OUT^w over OUT^+ comes at the cost of a 20% higher energy consumption.

Now, instead of deriving a node-specific path loss exponent, η_n in (2), to estimate the fade level of the link-channel pairs, we derive a global path loss exponent for all the nodes, and we still apply the link-channel pairs selection procedure in Section III-B. This approach was applied (in an indoor localization context) in [12]. We name this modified version of the outdoor RTI method COM^+ . With COM^+ , 11.7% of the link-channel pairs are selected, i.e., $\vartheta_e = 88.3\%$, and the false alarm rate is 0.06% (two triggered false alarms, person detected in the deployment area for 16 s). The RMSEs are $\bar{e}_m = 5.0$ m and $\bar{e}_s = 4.2$ m. Thus, deriving a global path loss exponent decreases the localization accuracy of the system by approximately 30% compared to deriving one for each node.

Finally, in a version we name COM^w , we still derive a global path loss exponent (as in COM^+), but this time we apply the weighted average approach in (19) for estimating the change in RSS of the links. With COM^w , the false alarm rate is 0.07% (two triggered false alarms, person detected in the deployment area for 17 s), the percentage of selected link-channel pairs is 31.3%, i.e., $\vartheta_e = 68.7\%$, and the RMSEs are $\bar{e}_m = 4.9$ m and $\bar{e}_s = 4.1$ m. Results and characteristics of the outdoor RTI methods discussed above are summarized in Table II.

C. Comparison with Previous RTI Methods

We now evaluate the performance of the state-of-the-art RTI methods in [5] and [12] on the same RSS measurements used to derive the results in Section VI-A. Both methods were developed for stationary indoor environments. Thus, in order to fairly evaluate their performance, we adapt both methods to nonstationary outdoor environments by applying the reference RSS estimation method in Section III-C and the people detection and tracking method in Section III-F.

Consider the method in [12]. The width λ of the elliptical sensitivity area of the link-channel pairs of the network depends on both the fade level and the sign of the measured change in RSS. The fade level is estimated by deriving a global path loss exponent for all the nodes. The RSS variance of the link-channel pairs estimated in stationary conditions is not taken into consideration. We refer to this method as *fade level-based*, or FLB , and consider three different versions:

TABLE III
SUMMARY OF THE PERFORMANCE OF PREVIOUS RTI METHODS

METHOD	ϑ_e	False alarm rate [%]	\bar{e}_m [m]	\bar{e}_s [m]
FLB^U	0.0	0.74	4.3	4.1
FLB^w	55.0	0.89	6.1	7.2
FLB^+	83.1	1.41	7.2	8.6
RFL^p	25.0	0.92	5.6	6.9
RFL^f	50.0	0.95	5.6	6.5
RFL^+	78.8	1.19	6.1	7.3

FLB^U : all the link-channel pairs are selected.

FLB^w : the link-channel pairs with an average RSS, estimated in stationary conditions, lower than Υ_r are discarded. Among the remaining ones, only the link-channel pairs having positive fade level are selected. The weighted average approach in (19) is applied.

FLB^+ : the link-channel pairs with an average RSS, estimated in stationary conditions, lower than Υ_r are discarded. For each link, only the frequency channel with the maximum fade level is selected.

The results are listed in Table III. Differently than with the outdoor RTI method, the localization accuracy of the FLB method in [12] decreases when fewer link-channel pairs are selected. This makes the FLB method less energy-efficient than the proposed outdoor RTI method. Moreover, even when all the link-channel pairs are considered, as with FLB^U , the localization accuracy is approximately 20% lower than with OUT^+ , which uses only 12.8% of the link-channel pairs. In comparison, with FLB^+ , i.e., the most energy efficient version using only 16.9% of the link-channel pairs, the localization accuracy is approximately 125% worse than with the corresponding outdoor method OUT^+ . As far as the false alarm rate is concerned, the three considered versions of the method in [12] have a considerably worse performance than the proposed outdoor RTI method: the false alarm rate is 0.74% with FLB^U (12 triggered false alarms, person detected in the monitored area for more than three minutes), and 1.41% with FLB^+ (27 triggered false alarms, person detected in the monitored area for approximately six minutes). These results demonstrate that the method in [12] is prone to trigger several false alarms in a time-varying and multipath-rich outdoor environment due to the significant noise in the RSS measurements introduced by environmental factors.

We now consider the RTI method in [5]. There, the *relative* fade level of a link-channel pair $\{l, c\}$ is estimated as the difference between its average RSS estimated in stationary conditions, $\bar{r}_{l,c}$ and the lowest average RSS measured on the

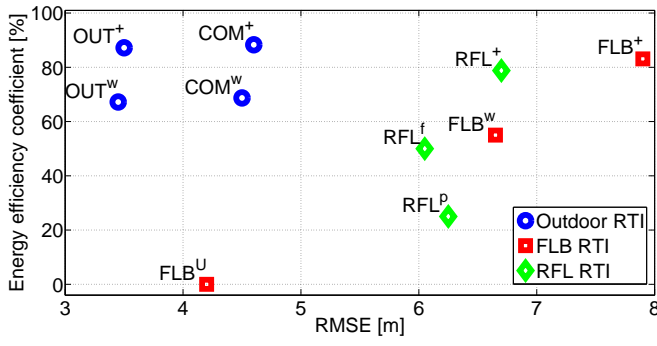


Fig. 6. Comparison of the performance of the considered RTI methods, in terms of localization accuracy and energy efficiency. The RMSE reported in the plot is computed as the average of \bar{e}_s and \bar{e}_m .

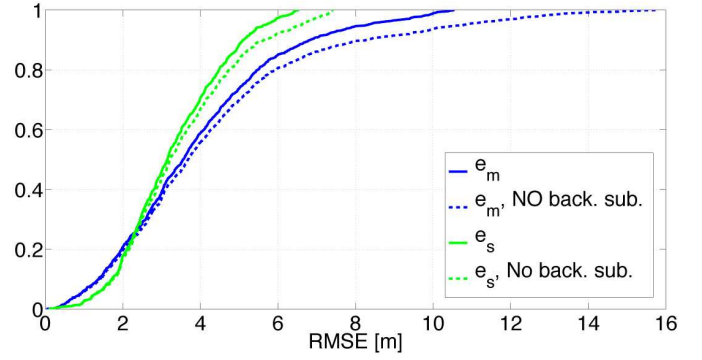


Fig. 7. Cumulative distribution functions of \bar{e}_s and \bar{e}_m of the novel outdoor RTI method (OUT^+), both when the background subtraction algorithm detailed in Section III-E is applied (solid lines) or not applied (dashed lines).

frequency channels in \mathcal{C} :

$$F_{l,c} = \bar{r}_{l,c} - \min_{c \in \mathcal{C}} \bar{r}_{l,c}. \quad (20)$$

Thus, $F_{l,c} \geq 0$, and $F_{l,c} = 0$ for one channel on each link. The RSS variance of the link-channel pairs estimated in stationary conditions is not taken into consideration. We refer to the RTI method in [5] as *relative fade level*, or *RFL*, and consider three different versions:

RFL^p: the link-channel pairs with $F_{l,c} > 0$ are selected. The change in RSS of the links is estimated by applying the weighted average approach in (19).

RFL^f: the link-channel pairs with an average RSS, measured in stationary conditions, lower than Υ_r are discarded. Among the remaining ones, the link-channel pairs with $F_{l,c} > 0$ are selected. The weighted average approach in (19) is applied.

RFL⁺: the link-channel pairs with an average RSS, measured in stationary conditions, lower than Υ_r are discarded. For each link, only the frequency channel with the maximum fade level is selected.

The results are summarized in Table III. Despite selecting more link-channel pairs, the three considered versions of the method in [5] have a localization accuracy from 73% (with *RFL^f*) to 91% (with *RFL⁺*) worse than that of the most energy efficient outdoor RTI method *OUT⁺*. In addition, the method in [5] has a significantly higher false alarm rate (0.92% with *RFL^p*, 0.95% with *RFL^f*, 1.19% with *RFL⁺*) than the proposed outdoor RTI method (0.04% with *OUT⁺*).

D. Background Subtraction Contribution

We now analyze the effects of the background subtraction algorithm detailed in Section III-E on the localization accuracy of the outdoor RTI method (*OUT⁺*). Figure 7 shows the cumulative distribution functions of \bar{e}_s and \bar{e}_m , both when background subtraction is applied (solid lines) or not applied (dashed lines). Background subtraction increases the robustness of the motion detection and localization process to the RSS variation due to environmental factors, which would introduce spurious blobs in the estimated radio tomographic images. Consequently, by applying the background subtraction

algorithm, the RTI system is overall more accurate, and does not incur in very high (*i.e.*, above 10 m) localization errors when links located far away from the current position of the target are affected by a consistent environmental noise.

E. Sensitivity Analysis

We analyze the effect of three parameters in Table I on the localization accuracy of the system. Figure 8 shows how \bar{e}_m and \bar{e}_s are affected by λ , *i.e.*, the width of the elliptical sensitivity area of the links, T_w , *i.e.*, the length of the time window used to determine the reference RSS of the links, and T_b , *i.e.*, the length of the background image training period. Simulations are performed by post-processing the RSS measurements collected during the deployment of the system when the person was located inside the monitored area. In the simulations, we set $T_w = T_b$. The results in Figure 8 indicate that the proposed outdoor RTI method is robust to variations of the three considered parameters, as both \bar{e}_m and \bar{e}_s have a 12% maximum variation from the values reported in table II.

F. System Lifetime

Finally, we evaluate the impact of the novel outdoor RTI method *OUT⁺* on the projected lifetime of the system. The parameter driving the energy consumption of the nodes is the radio duty cycle, that depends on which link-channel pairs are selected for RTI. As detailed in Algorithm 1, every ΔT_N hours the system measures all the link-channel pairs of the network for ΔT_c minutes. At the end of this period, the most reliable link-channel pairs are selected. The projected lifetime of the system is estimated as the time elapsed until a node runs out of power.

We use the Monte Carlo method: in each simulation, every ΔT_N hours, the weights $\rho_{l,c}$ in (5) that were calculated during the real deployment of the system are randomly re-assigned to the link-channel pairs of the network. Based on this re-assignment, a new set \mathcal{L} of link-channel pairs to be used for RTI is defined every ΔT_N hours. We assume that the nodes are equipped with *D*-type alkaline batteries having an 18 Ah capacity. However, we do not take into consideration the effect

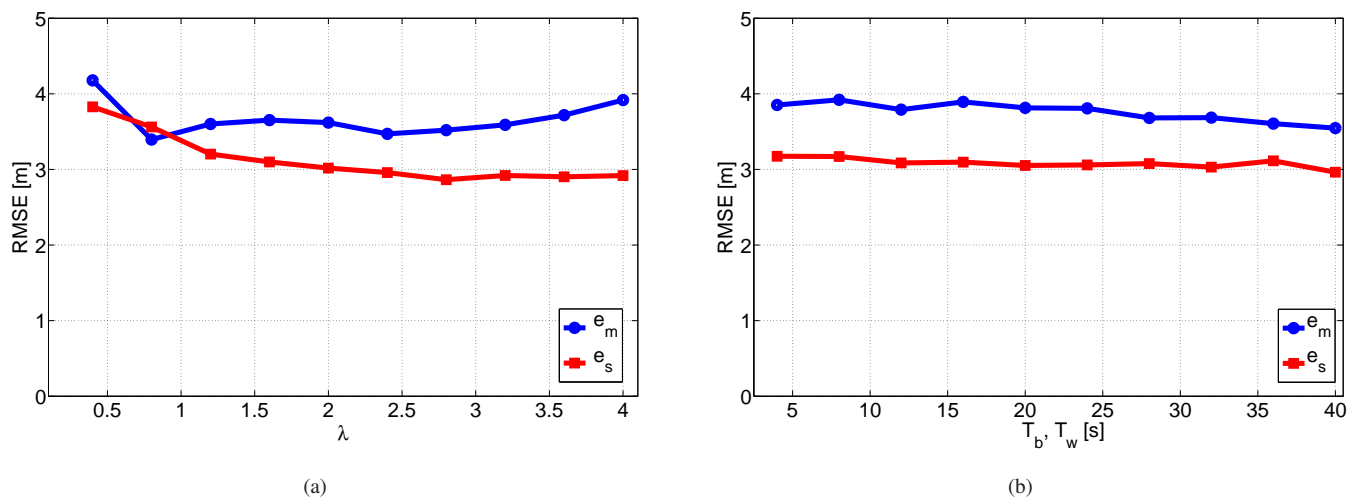


Fig. 8. Results of the sensitivity analysis of the energy-efficient outdoor RTI method (OUT^+). In (a), the localization accuracy of the system with different values of λ , *i.e.*, the width of the elliptical sensitivity area of the links. In (b), we modify the length of the time window used to determine the reference RSS of the links (T_w) and the length of the background image training period (T_b).

of environmental factors such as *e.g.* temperature changes on the battery discharge characteristics [45].

The results of the simulations are in Figure 9. We analyze the three most accurate RTI methods among the ones taken into consideration, *i.e.*, OUT^+ , OUT^w , and FLB^U . The method FLB^U [12], which continuously measures all the link-channel pairs of the network, grants a projected lifetime of approximately 24 days. In Figure 9(a), with $\Delta T_c = 5$ minutes, we progressively increase the value of ΔT_N from 1 hour to 24 hours. In (b), with $\Delta T_N = 2$ hours, we progressively increase the value of ΔT_c from 1 minute to 15 minutes. Each time, we perform 1000 simulations. The solid lines in the plots represent the median projected system lifetime of the simulations, the two edges the 25th and 75th percentiles of the distribution. OUT^+ extends the projected lifetime of the system to 104 days when $\Delta T_N = 1$ and 139 days when $\Delta T_N = 24$ hours, further enhancing the projected lifetime of OUT^w (58 days and 64 days, respectively). The projected system lifetime is influenced also by the length of the evaluation period ΔT_c , as shown in Figure 9(b). The impact of this parameter is more evident with OUT^+ , which at run-time uses a smaller percentage of link-channel pairs than OUT^w . Setting ΔT_c to a small value would further extend the lifetime of the system. A larger ΔT_c grants a more reliable evaluation of the characteristics (*i.e.*, fade level and sensitivity to the environmental noise) of the link-channel pairs, which severely affects the detection and localization performance of the RTI system.

Finally, in Figure 10 we show the RMSE (both when the person is moving and stationary) obtained by processing the RSS measurements collected during the deployment of the system with the outdoor RTI method OUT^+ , when the value of ΔT_N is progressively increased from 15 minutes to 6 hours ($\Delta T_c = 5$ minutes). The results demonstrate that the localization accuracy can be further increased by triggering more frequently the procedure of evaluation and selection of the link-channel pairs to be used for RTI. We observe that the

reduction in the localization error is limited to approximately 0.6 m, while the reduction of the lifetime of the system lifetime would approximately be 30 days.

In this section, we did not assess the effect of the position of the RF sensors on the lifetime of the system. Different sensor positions during the deployment phase would have modified the fade level of the link-channel pairs. As a consequence, the selection procedure described in Section III-B would have generated a different set of link-channel pairs to be considered for RTI, altering the energy consumption of the nodes. The work in [44] showed that even small-scale changes (*i.e.*, in the order of the wavelength) in the position of the RF sensors have a significant impact on the performance of an RTI system. In that work different methods to select *sub-optimal* positions have been introduced for the purpose of optimizing the overall fade level of the network, thus the localization accuracy. Similar deployment schemes could be applied also in an outdoor scenario. The work in [46] proposed a stochastic model of human-induced fading to derive closed-form fundamental limits to the localization accuracy of a RF sensor network. We leave this aspect to future works.

VII. CONCLUSION

In this paper, we present and evaluate a novel RTI method for accurately detecting and tracking people in nonstationary outdoor environments. An RTI system is composed of static RF sensors, communicating on multiple frequency channels in the 2.4 GHz ISM band, which continuously measure the RSS of the links of the mesh network to estimate the change in the electromagnetic field of the monitored area introduced by the presence and movements of people. The outdoor RTI method described in this work makes the system robust to the time-varying environmental noise typical of harsh outdoor environments, *i.e.*, the variation in RSS introduced by environmental factors such as wind-driven foliage, rainfalls, or snow. In addition, the proposed method improves the energy efficiency of the system by selecting only link-channel pairs which are

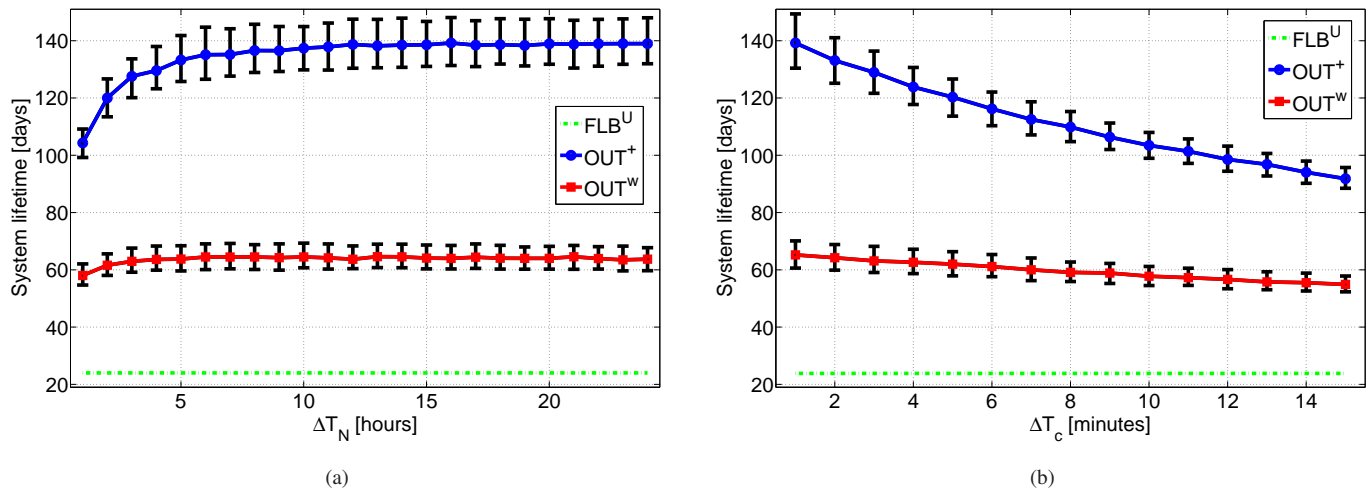


Fig. 9. Results of simulations of the projected lifetime of the system with OUT^+ , OUT^w , and FLB^U . In (a), with $\Delta T_c = 5$ minutes, ΔT_N is progressively increased from 1 hour to 24 hours. In (b), with $\Delta T_N = 2$ hours, ΔT_c is progressively increased from 1 minute to 15 minutes. Each time, 1000 simulations are performed. We assume that the nodes are equipped with D -type alkaline batteries having an 18 Ah capacity. The solid lines in the plots represent the median projected system lifetime of the simulations, the two edges the 25th and 75th percentiles of the distribution.

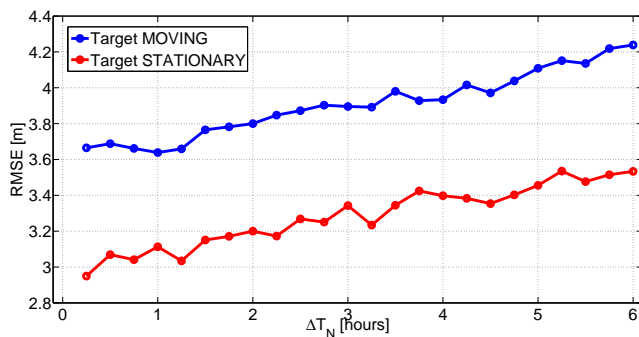


Fig. 10. The RMSE, when the target is moving (blue line) or is stationary (red line), obtained processing the RSS measurements collected during the deployment of the RTI system when ΔT_N is progressively increased from 15 minutes to 6 hours ($\Delta T_c = 5$ minutes).

reliable indicators of the presence of a person on the link line. To experimentally verify the performance of the outdoor RTI method, we deploy a RTI system in a large forested area. The results demonstrate that the novel outdoor RTI method minimizes the false alarm rate and reduces significantly the localization error (from 20% to 46%) and energy consumption (from 62% to 87%) compared to already existing indoor RTI methods, which we suitably adapted to the considered outdoor scenario to grant a fair comparison.

In future works, we will improve the energy efficiency of the RTI system by applying area coverage criteria to further reduce the set of selected link-channel pairs and by adaptively tuning the sampling frequency of the system based on the observed environmental conditions. In addition, we will investigate the robustness to environmental noise of other frequency bands (e.g., 433 MHz and 900 MHz).

ACKNOWLEDGMENTS

This work is supported by the U.S. National Science Foundation under Grant Nos. 1035565 and 1407949, and supported by the U.S. Department of Homeland Security under a S&T SBIR FY13.1 award.

REFERENCES

- [1] N. Patwari and J. Wilson, "Rf sensor networks for device-free localization: Measurements, models, and algorithms," *Proceedings of the IEEE*, vol. 98, no. 11, pp. 1961–1973, Nov 2010.
- [2] J. Wilson and N. Patwari, "Radio tomographic imaging with wireless networks," *Mobile Computing, IEEE Transactions on*, vol. 9, no. 5, pp. 621–632, May 2010.
- [3] O. Kaltiokallio, M. Bocca, and N. Patwari, "Enhancing the accuracy of radio tomographic imaging using channel diversity," in *Mobile Adhoc and Sensor Systems (MASS), 2012 IEEE 9th International Conference on*, Oct 2012, pp. 254–262.
- [4] C. Anderson, R. Martin, T. Walker, and R. Thomas, "Radio tomography for roadside surveillance," *Selected Topics in Signal Processing, IEEE Journal of*, vol. 8, no. 1, pp. 66–79, Feb 2014.
- [5] M. Bocca, O. Kaltiokallio, N. Patwari, and S. Venkatasubramanian, "Multiple target tracking with RF sensor networks," *Mobile Computing, IEEE Transactions on*, vol. 13, no. 8, pp. 1787–1800, Aug 2014.
- [6] O. Kaltiokallio, M. Bocca, and N. Patwari, "Follow @grandma: Long-term device-free localization for residential monitoring," in *Local Computer Networks Workshops (LCN Workshops), 2012 IEEE 37th Conference on*, Oct 2012, pp. 991–998.
- [7] K. Srinivasan, P. Dutta, A. Tavakoli, and P. Levis, "Understanding the causes of packet delivery success and failure in dense wireless sensor networks," in *Proceedings of the 4th International Conference on Embedded Networked Sensor Systems*, ser. SenSys '06. New York, NY, USA: ACM, 2006, pp. 419–420. [Online]. Available: <http://dx.doi.org/10.1145/1182807.1182885>
- [8] S. Basagni, M. Y. Naderi, C. Petrioli, and D. Spensa, "Wireless sensor networks with energy harvesting," in *Mobile Ad Hoc Networking*. John Wiley & Sons, Inc., 2013, pp. 701–736. [Online]. Available: <http://dx.doi.org/10.1002/978111851118511305.ch20>
- [9] Reuters. Kenya to use drones to fight elephant, rhino poachers. [Online]. Available: <http://www.reuters.com/article/2014/03/25/us-kenya-poaching-idUSBREA201D020140325>
- [10] Z. Butler, P. Corke, R. Peterson, and D. Rus, "From robots to animals: Virtual fences for controlling cattle," *Int. J. Rob. Res.*, vol. 25, no. 5-6, pp. 485–508, May 2006. [Online]. Available: <http://dx.doi.org/10.1177/0278364906065375>

- [11] J. Wilson and N. Patwari, "A fade-level skew-laplace signal strength model for device-free localization with wireless networks," *Mobile Computing, IEEE Transactions on*, vol. 11, no. 6, pp. 947–958, June 2012.
- [12] O. Kaltiokallio, M. Bocca, and N. Patwari, "A fade level-based spatial model for radio tomographic imaging," *Mobile Computing, IEEE Transactions on*, vol. 13, no. 6, pp. 1159–1172, June 2014.
- [13] X. Huang, R. Janaswamy, and A. Ganz, "Scout: Outdoor localization using active rfid technology," in *Broadband Communications, Networks and Systems, 2006. BROADNETS 2006. 3rd International Conference on*, Oct 2006, pp. 1–10.
- [14] R. Cucchiara, M. Fornaciari, A. Prati, and P. Santinelli, "Mutual calibration of camera motes and rfids for people localization and identification," in *Proceedings of the Fourth ACM/IEEE International Conference on Distributed Smart Cameras*, ser. ICDS'10. New York, NY, USA: ACM, 2010, pp. 65–72. [Online]. Available: <http://doi.acm.org/10.1145/1865987.1865998>
- [15] Soro S. and Heinzelman W., "A survey of visual sensor networks," *Advances in Multimedia*, 2009.
- [16] D. Tahmouh and J. Silvius, "Remote detection of humans and animals," in *Applied Imagery Pattern Recognition Workshop (AIPRW), 2009 IEEE*, Oct 2009, pp. 1–8.
- [17] Tahmouh, D. and Silvius, J., "Radar measurement of human polarimetric micro-doppler," *JECE*, vol. 2013, pp. 11:11–11:11, Jan. 2013. [Online]. Available: <http://dx.doi.org/10.1155/2013/804954>
- [18] R. Lane and S. Hayward, "Detecting personnel in wooded areas using mimo radar," in *Radar Systems, 2007 IET International Conference on*, Oct 2007, pp. 1–5.
- [19] K. Bannister, G. Giorgetti, and S. Gupta, "Wireless sensor networking for hot applications: Effects of temperature on signal strength, data collection and localization," in *Proceedings of the 5th Workshop on Embedded Networked Sensors (HotEmNets 08)*, 2008.
- [20] R. Marfievici, A. Murphy, G. Picco, F. Ossi, and F. Cagnacci, "How environmental factors impact outdoor wireless sensor networks: A case study," in *Mobile Ad-Hoc and Sensor Systems (MASS), 2013 IEEE 10th International Conference on*, Oct 2013, pp. 565–573.
- [21] M. Hashim and S. Stavrou, "Measurements and modelling of wind influence on radiowave propagation through vegetation," *Wireless Communications, IEEE Transactions on*, vol. 5, no. 5, pp. 1055–1064, May 2006.
- [22] J. Wilson and N. Patwari, "See-through walls: Motion tracking using variance-based radio tomography networks," *Mobile Computing, IEEE Transactions on*, vol. 10, no. 5, pp. 612–621, May 2011.
- [23] O. Kaltiokallio and M. Bocca, "Real-time intrusion detection and tracking in indoor environment through distributed rssi processing," in *Embedded and Real-Time Computing Systems and Applications (RTCSA), 2011 IEEE 17th International Conference on*, vol. 1, Aug 2011, pp. 61–70.
- [24] Y. Zhao, N. Patwari, J. M. Phillips, and S. Venkatasubramanian, "Radio tomographic imaging and tracking of stationary and moving people via kernel distance," in *Proceedings of the 12th International Conference on Information Processing in Sensor Networks*, ser. IPSN '13. New York, NY, USA: ACM, 2013, pp. 229–240. [Online]. Available: <http://doi.acm.org/10.1145/2461381.2461410>
- [25] Y. Zhao and N. Patwari, "Noise reduction for variance-based device-free localization and tracking," in *Sensor, Mesh and Ad Hoc Communications and Networks (SECON), 2011 8th Annual IEEE Communications Society Conference on*, June 2011, pp. 179–187.
- [26] M. A. Kanso and M. G. Rabbat, "Compressed rf tomography for wireless sensor networks: Centralized and decentralized approaches," in *Proceedings of the 5th IEEE International Conference on Distributed Computing in Sensor Systems*, ser. DCOSS '09. Berlin, Heidelberg: Springer-Verlag, 2009, pp. 173–186. [Online]. Available: http://dx.doi.org/10.1007/978-3-642-02085-8_13
- [27] M. Khaledi, S. Kaser, N. Patwari, and M. Bocca, "Energy efficient radio tomographic imaging," in *Sensor, Mesh and Ad Hoc Communications and Networks (SECON), 2014 11th Annual IEEE Communications Society Conference on*, June-July 2014 (to appear).
- [28] N. Patwari and P. Agrawal, "Effects of correlated shadowing: Connectivity, localization, and rf tomography," in *Information Processing in Sensor Networks, 2008. IPSN '08. International Conference on*, April 2008, pp. 82–93.
- [29] P. Agrawal and N. Patwari, "Correlated link shadow fading in multi-hop wireless networks," *Wireless Communications, IEEE Transactions on*, vol. 8, no. 8, pp. 4024–4036, August 2009.
- [30] T. Rappaport, *Wireless Communications: Principles and Practice*, 2nd ed. Upper Saddle River, NJ, USA: Prentice Hall PTR, 2001.
- [31] D. Lymberopoulos, Q. Lindsey, and A. Savvides, "An empirical characterization of radio signal strength variability in 3-d ieee 802.15.4 networks using monopole antennas," in *Wireless Sensor Networks*, ser. Lecture Notes in Computer Science, K. Rmer, H. Karl, and F. Mattern, Eds. Springer Berlin Heidelberg, 2006, vol. 3868, pp. 326–341. [Online]. Available: http://dx.doi.org/10.1007/11669463_24
- [32] J. Vallet, O. Kaltiokallio, M. Myrsky, J. Saarinen, and M. Bocca, "Simultaneous rssi-based localization and model calibration in wireless networks with a mobile robot," in *ANT/MobiWIS*, 2012, pp. 1106–1113.
- [33] K. Srinivasan and P. Levis, "Rssi is under appreciated," in *In Proceedings of the Third Workshop on Embedded Networked Sensors (EmNets)*, 2006.
- [34] M. Ceriotti, M. Chini, A. L. Murphy, G. P. Picco, F. Cagnacci, and B. Tolhurst, "Motes in the jungle: Lessons learned from a short-term wsn deployment in the ecuador cloud forest," in *Proceedings of the 4th International Conference on Real-world Wireless Sensor Networks*, ser. REALWSN'10. Berlin, Heidelberg: Springer-Verlag, 2010, pp. 25–36. [Online]. Available: <http://dl.acm.org/citation.cfm?id=1947841.1947845>
- [35] C. R. Vogel, *Computational Methods for Inverse Problems*. Philadelphia, PA, USA: Society for Industrial and Applied Mathematics, 2002.
- [36] M. Piccardi, "Background subtraction techniques: a review," in *Systems, Man and Cybernetics, 2004 IEEE International Conference on*, vol. 4, Oct 2004, pp. 3099–3104 vol.4.
- [37] Y. Benezeth, P.-M. Jodoin, B. Emile, H. Laurent, and C. Rosenberger, "Review and evaluation of commonly-implemented background subtraction algorithms," in *Pattern Recognition, 2008. ICPR 2008. 19th International Conference on*, Dec 2008, pp. 1–4.
- [38] Texas Instruments. A USB-Enabled system-on-chip solution for 2.4 GHz IEEE 802.15.4 and ZigBee applications. [Online]. Available: <http://www.ti.com/lit/ds/symlink/cc2531.pdf>
- [39] Texas Instruments. 2.4 GHz Inverted F Antenna. [Online]. Available: <http://www.ti.com/lit/an/swru120b/swru120b.pdf>
- [40] M. Bocca, O. Kaltiokallio, and N. Patwari, "Radio tomographic imaging for ambient assisted living," in *Evaluating AAL Systems Through Competitive Benchmarking*, ser. Communications in Computer and Information Science, S. Chessa and S. Knauth, Eds. Springer Berlin Heidelberg, 2013, vol. 362, pp. 108–130. [Online]. Available: http://dx.doi.org/10.1007/978-3-642-37419-7_9
- [41] P. Sigrist, P. Coppin, and M. Hermy, "Impact of forest canopy on quality and accuracy of gps measurements," *International Journal of Remote Sensing*, vol. 20, no. 18, pp. 3595–3610, 1999. [Online]. Available: <http://dx.doi.org/10.1080/014311699211228>
- [42] A. Bastos and H. Hasegawa, "Behavior of gps signal interruption probability under tree canopies in different forest conditions," *European Journal of Remote Sensing*, vol. 46, pp. 613–622, Oct. 2013.
- [43] C. Alippi, *Intelligence for Embedded Systems: A Methodological Approach*, 1st ed. Springer, 2014.
- [44] M. Bocca, A. Luong, N. Patwari, and T. Schmid, "Dial it in: Rotating RF sensors to enhance radio tomography," in *Sensing, Communication, and Networking (SECON), 2014 Eleventh Annual IEEE International Conference on*, June 2014, pp. 600–608.
- [45] C. Park, K. Lahiri, and A. Raghunathan, "Battery discharge characteristics of wireless sensor nodes: an experimental analysis," in *Sensor and Ad Hoc Communications and Networks, 2005. IEEE SECON 2005. 2005 Second Annual IEEE Communications Society Conference on*, Sept 2005, pp. 430–440.
- [46] V. Rampa, S. Savazzi, M. Nicoli, and M. D'Amico, "Physical modeling and performance bounds for device-free localization systems," *Signal Processing Letters, IEEE*, vol. 22, no. 11, pp. 1864–1868, Nov 2015.